Original Article

Targeting STT3A produces an anti-tumor effect in lung adenocarcinoma by blocking the MAPK and PI3K/AKT signaling pathway

Jiahan Cheng[1#], Liang Xia[1#], Xiaohu Hao[1#], Fanyi Gan[1], Yuquan Bai[1], Chuanfen Zhang[1], Yonghong Mao[1], Yunke Zhu[1], Qiang Pu[1], Dong Won Park[2], Simona Tavolari[3,4], Jiandong Mei[1], Yaohui Chen[1], Senyi Deng[1], Lunxu Liu[1]

[1]Institute of Thoracic Oncology and Department of Thoracic Surgery, West China Hospital, Sichuan University, Chengdu, China; [2]Department of Internal Medicine, Hanyang University College of Medicine, Seoul, Korea; [3]Division of Medical Oncology, IRCCS Azienda Ospedaliero-Universitaria of Bologna, Bologna, Italy; [4]Department of Experimental, Diagnostic and Specialty Medicine, University of Bologna, Bologna, Italy

Contributions: (I) Conception and design: L Liu, S Deng, Y Chen; (II) Administrative support: S Deng, L Liu; (III) Provision of study materials or patients: L Liu, Y Zhu, Q Pu, J Mei; (IV) Collection and assembly of data: J Cheng, L Xia; (V) Data analysis and interpretation: All authors; (VI) Manuscript writing: All authors; (VII) Final approval of manuscript: All authors.

[#]These authors contributed equally to this work.

Correspondence to: Lunxu Liu, MD, PhD; Senyi Deng, PhD; Yaohui Chen, PhD. Institute of Thoracic Oncology and Department of Thoracic Surgery, West China Hospital, Sichuan University, No. 37 Guoxue Alley, Wuhou District, Chengdu 610041, China. Email: lunxu_liu@aliyun.com; senyi_deng@scu.edu.cn; YHChen@scu.edu.cn.

Background: Glycosylation is crucial for the stability and biological functions of proteins. The aberrant glycosylation of critical proteins plays an important role in multiple cancers, including lung adenocarcinoma (LUAD). STT3 oligosaccharyltransferase complex catalytic subunit A (STT3A) is a major isoform of N-linked glycosyltransferase that catalyzes the glycosylation of various proteins. However, the functions of STT3A in LUAD are still unclear.

Methods: The expression profiles of STT3A were initially analyzed in public data sets and then validated by quantitative real-time polymerase chain reaction, Western blot and immunohistochemistry assays in clinical LUAD samples. The overall survival (OS) between patients with high and low STT3A expression was compared using a Kaplan-Meier curve with a log-rank analysis. STT3A was knocked-out using CRISPR/Cas9 and inhibited by NGI-1. Cell Counting Kit-8, colony formation assay, wound-healing, transwell assay, and flow cytometry were performed to assess the cellular functions of STT3A *in vitro*. A mice xenograft model was established to investigate the effects of STT3A on tumor growth *in vivo*. Further, the downstream signaling pathways of STT3A were screened by mass spectrometry with a bioinformatics analysis, and the activation of the target pathways were subsequently validated by Western blot.

Results: The expression of STT3A was frequently upregulated in LUAD tissues than normal lung tissues. The high expression of STT3A was significantly associated with poor OS in LUAD patients. The knockout or inhibition of STT3A suppressed proliferation, migration, and invasion, and arrested the cell cycle of LUAD cell lines *in vitro*. Similarly, the knockout or inhibition of STT3A suppressed tumor growth *in vivo*. In terms of molecular mechanism, STT3A may promote LUAD progression by activating the mitogen-activated protein kinase (MAPK) and phosphatidylinositol-3-kinase and protein kinase B (PI3K/AKT) pathways and regulating the epithelial-mesenchymal transition.

Conclusions: STT3A promotes LUAD progression via the MAPK and PI3K/AKT signaling pathways and could serve as a novel prognostic biomarker and potential therapeutic target for LUAD patients.

Keywords: STT3 oligosaccharyltransferase complex catalytic subunit A (STT3A); glycosylation; lung adenocarcinoma; MAPK/ERK pathway; phosphatidylinositol-3-kinase and protein kinase B pathway (PI3K/AKT pathway)

Submitted Mar 02, 2022. Accepted for publication Jun 17, 2022.
doi: 10.21037/tlcr-22-396
View this article at: https://dx.doi.org/10.21037/tlcr-22-396

Introduction

Lung cancer is one of the most frequently diagnosed malignances worldwide and is the primary leading cause of cancer-related deaths, accounting for approximately 25% of all deaths (1). The advent of novel treatments, particularly checkpoint immunotherapy and targeted therapy, has led to a decline in the mortality of lung cancer patients (2). As the molecular characterization and genetic alterations of lung cancer are still not completely understood, many patients fail to respond to the current approaches or standard clinical management; thus, underlying potential therapeutic targets need to be identified to increase the survival of these patients.

Protein glycosylation is thought to have an essential and functional effect during protein post-translational modifications (PTMs), and serves multiple biological activities, including cell recognition, cell-cell interactions, signaling, and transformation. Glycans affect the properties of protein folding, synthesis, conjugates, conformation, and stability (3-5). Previous studies have shown that protein glycosylation is involved in the progression of almost all cancer types and could serve as a novel target for potential therapeutics in cancer treatment (6-8). Thus, we speculated the glycosyltransferases, which are key enzymes in glycan modification, could provide novel targets for cancer therapy.

To date, research has shown that N-glycosylation determines protein functions and activities, and plays a critical role in biological processes (BPs), including tumorigenesis (9,10). N-glycosylation is initiated in the lumen of the endoplasmic reticulum (ER), in which oligosaccharyltransferase (OST), a central enzyme in this protein modification reaction, catalyzes the transfer of a well-defined oligosaccharide donor substrate (11,12). Notably, the STT3 oligosaccharyltransferase complex catalytic subunit A (STT3A) is a subunit of OST complexes in mammals and is mainly responsible for the co-translational glycosylation of the nascent polypeptide(13). Preliminary research suggests that epithelial-mesenchymal transition (EMT) enriches the upregulation of programmed death-ligand 1 (PD-L1) expression and STT3A recruitment via β-catenin, and STT3A plays a critical role in PD-L1 induction by regulating PD-L1 glycosylation and protein stabilization, allowing the evasion of immune surveillance (14). Driven by the interlukin-6 (IL-6)/Janus kinase 1 (JAK1) pathway, the phosphorylation of the PD-L1 Tyr112 subsequently recruits the ER-associated N-glycosyltransferase isoform STT3A, which enhances PD-L1 glycosylation and maintains PD-L1 stability and assists cancer cells to evade immune surveillance (15). Collectively, these studies suggest that STT3A contributes to the development of tumors at the cellular level; however, it is not yet known how STT3A directly functions in lung adenocarcinoma (LUAD).

In this study, we compared the levels of N-glycosyltransferase STT3A expression in LUAD tissues based on The Cancer Genome Atlas (TCGA) database. Further experiments revealed its molecular functions in relation to cell proliferation, migration, and invasion, and its potential regulatory mechanism. The study also examined the biological changes caused by STT3A overexpression in LUAD cells, which may provide novel insights into therapeutic targets for LUAD. We present the following article in accordance with the ARRIVE reporting checklist (available at https://tlcr.amegroups.com/article/view/10.21037/tlcr-22-396/rc).

Methods

Clinical samples

Patients who were diagnosed with LUAD and had not undergone any radiotherapy or chemotherapy before surgery were selected for this study. Fresh-frozen and paraffin-embedded tissues from 10 patients with matched adjacent normal tissues were collected at the West China Hospital, Sichuan University between August 3rd, 2020 and August 14, 2020.

To evaluate the correlation of STT3A expression with the prognosis of LUAD patients, 183 tissue microarray (TMA) samples were obtained from the Shanghai Outdo Biotech CO., Ltd. (China). Data on patients' clinical demographics, such as their gender, age, tumor size, pathological grade, lymph node metastasis status, histology TNM stage, overall survival (OS) time, and survival status, were also collected. The study was conducted in accordance with the Declaration of Helsinki (as revised in 2013). The study was approved by the Ethics Committee of the West

China Hospital, Sichuan University (No. 2021-1746). Informed consent of patients was waived for this study after the approval of the ethics committee.

Cell culture

The LUAD cell lines (A549, PC9, H1299, HCC78, HCC827, H3122 and H1975), human bronchial epithelial cell lines (HBE, and MRC5), and HEK293 cell line were obtained from the Shanghai Academy of Science (Shanghai, China). The HEK293 cells were maintained in Dulbecco's modified eagle medium (Gibco, United States). The remaining cell lines were maintained in Roswell Park Memorial Institute Medium–1640 medium (Gibco, United States). All the media were supplemented with 10% fetal bovine serum (FBS; Gimini, United States), 1% penicillin, and streptomycin (Gibco, United States). All the cell lines were cultured at 37 ℃ with 5% carbon dioxide (CO_2) and then passaged for less than 2 months before being renewed with frozen.

Plasmids and lentivirus

Briefly, the knockdown of STT3A was performed using sgSTT3A (STT3A-1 F: c accgAAGGTGGTACGTG ACGATGG, R: aaacCCATCGTCACGTACCACCTTc; STT3A-2F: caccgGAGTAGAAACGCCCCGTCCA, R: aaacTGGACGGGGCGTTTCTACTCc), and lentiCRISPRv2 plasmids (Zhang Lab), and compared to a negative control of sgNC encoding a non-specific 20 nt guide ribonucleic acid (RNA). The cells were then co-transfected with lentiCRISPRv2 plasmids with CRISPR/Cas9 sgRNA. Next, 2 days after the transfection, the cells were selected by puromycin for 1 week to obtain stable cell lines.

qRT-PCR

Total RNA was isolated from the frozen tissues using TRIzol reagent (Invitrogen, Carlsbad, CA, USA) in accordance with the manufacturer's instructions. PrimerScript RT Reagent Kit (Takara, Kumastu, Shiga, Japan) was used to synthesize the complementary deoxyribonucleic acid (cDNA), and a quantitative real-time polymerase chain reaction (qRT-PCR) analysis was performed via SYBR Premix Ex Taq TM II (Takara, Kumastu, Shiga, Japan). All the reactions were conducted on the CFX Connect Real-time system (Bio-Rad, Hercules, CA, USA). The relative quantification was normalized against the housekeeping gene glyceraldehyde-3-phosphate dehydrogenase and calculated using the $2^{-\Delta\Delta CT}$ method.

The forward primer sequence of STT3A was 5'-AACCCTGAGAGATATGGCTGG-3', and the reverse primer sequence was 5'-CAGACGAGTGGAGAAGGAT AATAC-3'). The forward primer sequence of GAPDH was 5'-GGAGCGATCCCTCCAAAAT-3', and the reverse primer sequence was 5'-GGCTCTTCTCATACTTCTCATGG-3').

Colony formation assay

The transfected PC-9 and H1299 cells were seeded in 6-well plates (1,000 cells per well) with culture medium for 2 weeks. The cells were washed twice with ice-phosphate buffered solution (PBS) and fixed with 4% paraformaldehyde for 30 mins, followed by 0.1% crystal violet staining for 15 min. The cells were then re-washed twice with ice-PBS and photographed with a digital camera.

Cell proliferation

To evaluate the proliferative activity of cells, a cell counting kit-8 (CCK-8; Beyotime, Shanghai, China) was used in accordance with the manufacturer's instructions. The cells were seeded into 96-well plates at a density of 3×10^3 cells per well. After the cells were adherent, an absorbance of 450 nm wavelength was used to measure cell proliferation via the microplate spectrophotometer (BioTEk, VT, USA) at 0 (baseline), 24, 48, 72, and 96 h.

Cell migration and invasion assays

For the wound-healing assay, the cells were seeded into 6-well plates until 90% confluence was reached. The plates were scratched with sterile 200-μL pipette tips and then washed 3 times with PBS to remove cell fragments. The cells were then maintained in serum-free medium at 37 ℃ and 5% CO_2. Images were taken at different time points (0, 24, and 48 h), and the wound distances were measured using ImageJ software.

For the Transwell assay, 5×10^4 transfected PC-9 or H1299 cells and their control cells in 200 μL of serum-free RPMI-1640 medium were seeded into the upper chambers of the Transwell inserts (Corning, Corning, NY, USA) with or without Matrigel. Next, 600 μL of PPMI-1640 medium containing 20% FBS was added to the lower chambers. After 24 h of incubation, the cells remaining in the upper chambers were removed with a cotton swab, and

those that had invaded the bottom surface were fixed with 75% ice-alcohol for 30 min and stained with 1% crystal violet solution for 20 min. An inverted microscope was then used for imaging. The invasion capability of the cells was evaluated in accordance with the standard protocol.

Cell-cycle and apoptosis assays

The cells were harvested at 90% confluence in 6-cm dishes and washed with ice-PBS buffer. After being fixed in 70% ethanol at 4 ℃ overnight, the cells were re-washed twice and then stained with propidium iodide (PI)/RNase Staining Solution (Beyotime, Shanghai, China) for 30 min away from light. The distribution of the cell-cycle phases was detected using a flow cytometer (cytoflex, Beckman, Germany). For the cell apoptosis assay, the cells were processed with a Annexin V-FITC Apoptosis Detection Kit (Beyotime, Shanghai, China), and examined by cell sorting in accordance with the manufacturer's instructions. Approximately 2×10^4 cells were collected for each experiment, and the assays were independently replicated 3 times.

Western blotting

The samples from the fresh-frozen tissues and cells were lysed in RIPA buffer (Solarbio, Beijing, China) with protease and phenylmethylsulfonyl fluoride inhibitor cocktails (Solarbio, Beijing, China). Protein concentration was determined using a bicinchoninic acid protein assay kit (Solarbio, Beijing, China). An equal amount of proteins (30 μg) for each sample were loaded on 10% sodium dodecyl sulfate–polyacrylamide gels and then transferred to polyvinylidene fluoride membranes (Merck Millipore, Cork, IRL). The membranes were subsequently blocked with tris buffered saline with tween containing 5% skim milk at room temperature for 1 h and incubated with diluted antibody at 4 ℃ overnight.

The following primary antibodies were used: rabbit anti-EGFR (1:1,000, CST, #4267); rabbit anti-PEGFR (1:1,000, CST, #3777); mouse anti-AKT (1:2,000, CST, #2920); rabbit anti-PAKT (1:2,000, CST, #4060); rabbit anti-ERK (1:2,000, CST, #4695); rabbit anti-PERK (1:1,000, CST, #4370); mouse anti-MEK (1:1,000, CST, #4694); rabbit anti-PMEK (1:1,000, CST, #9154); mouse anti-Tubulin (1:5,000, ZSGB-BIO, TA347064); mouse anti-E-cadherin (1:1,000, CST, #14472); rabbit anti-N-cadherin (1:1,000, CST, #13116); rabbit anti-vimentin (1:1,000, CST, #5741); rabbit anti-P21 (1:1,000, CST, #2947); rabbit anti-P27 (1:1,000, CST, #3686); rabbit anti-CDK4 (1:1,000, CST, #12790); and rabbit anti-CDK6 (1:1,000, CST, #13331).

IHC and quantification

Formalin-fixed and paraffin-embedded sections were re-warmed at 65 ℃ for 3 h before being deparaffinized and rehydrated. After being processed, the tissue sections were incubated with anti-STT3A rabbit antibody (1:300; Proteintech, #66581-1-Ig) overnight at 4 ℃. These tissue sections were then incubated with horseradish peroxidase-conjugated anti-rabbit antibody (1:1,000, ZSGB-BIO) at 37 ℃ for 15 min. The sections were then stained with DAB + substrate-chromogen solution (ZSGB-BIO, Beijing, China) at room temperature for 30 s followed by counterstaining with hematoxylin. Samples incubated with PBS instead of antibodies served as the negative control. The immune-stained results were independently scored by 2 researchers in a blinded fashion.

The expression levels of STT3A were evaluated based on both the staining intensity score and percentage of positive cells using a semi-quantitative scoring system (16). Under the system, 0 indicated negative staining, 1 indicated weak staining, 2 indicated moderate staining, and 3 indicated strong staining. The percentage of positive cells was quantified as 0 for ≤5% positive cells, 1 for 6–25%, 2 for 26–50%, 3 for 51–75%, and 4 for ≥76%. The immunoactivity score was calculated by multiplying the staining intensity score and the percentage of the positive cells. Based on the STT3A immunoreactivity score, the patients were divided into the following 2 subgroups: (I) a low-expression group (based on an immunoreactivity score <6); and (II) a high-expression subgroup (based on an immunoreactivity score ≥6).

Mass spectrometry (MS) analyses

In this project, 2 groups of pc-9-sgNC and PC-9-sgSTT3A cell samples were detected by 4-dimensional (4D) label-free quantitative protein MS; each group had 3 duplicate samples (Jingjie Ltd., China). The MS/MS data were searched against the Uniprot Human protein database (Homo_sapiens_9606_SP_20210721.fasta containing 20387 entries) using Maxquant (V1.6.15.0), and the data analysis was performed using R software (Proteome Software). Peptides and modified peptides were accepted if they passed the 1% false discovery rate threshold.

Experiments in vivo

A protocol was prepared before the study without registration. Animal experiments *in vivo* were approved by the Animal Ethics Committee of the West China Hospital, Sichuan University (No. 2021987A), in compliance with institutional guidelines for the care and use of animals. We purchased 6-week-old female BALB/c nude mice from GemPharmatech Co., Ltd. (Jiangsu, China). The mice were housed in facilities approved by the Animal Care and Use Committee of West China Hospital, Sichuan University. For the xenograft mouse model, 10 mice were subcutaneously injected with 100 μL of 5×10^6 PC-9-sgSTT3A cells into the right flank. For the control group, 10 mice were subcutaneously injected with 100 μL of 5×10^6 PC-9-sgNC cells into the left flank. Then, 7 days after the first injection, tumor volumes were measured 3 times a week for a total of 28 days. Tumor volume was calculated using the following formula: V (mm^3) = (π/6) *L*W^2, where L and W referred to the longest longitudinal and transverse diameters, respectively.

For the NGI-1 therapeutic experiment, 14 nude mice were randomized into 2 groups. Each nude mouse was subcutaneously injected with of 5×10^6 PC-9 cells into the left armpit. Then, 10 days after the inoculation, the mice were randomized to receive i.p. NGI-1 (20 mg/kg) in mixed solutions (dimethyl sulfoxide, polyethylene glycol 300, Tween-80, and PBS) or blank nanoparticles 3 times per week for a total of 8 doses. All the mice were sacrificed on day 34, and the transplanted tumors and adjacent normal tissues were harvested. The specimens were fixed in 10% formalin and sectioned for imaging, and the remaining tissues were stored in liquid nitrogen for further experiments.

Survival analysis

Based on TCGA database, a survival analysis was conducted using the "survival" and "survminer" of R packages (17). Survival curves were estimated using the Kaplan-Meier method, and the log-rank test was used to analyze OS. The survival analysis of the Gene Expression Omnibus (GEO) data was conducted through the Kaplan-Meier Plotter database website (https://kmplot.com/analysis/index.php?p=service&cancer=lung) (18). A survival analysis of the effects of differentially expressed (DE) glycosyltransferases expression levels on the prognosis of LUAD was conducted using TCGA data from the Gene Expression Profiling Interactive Analysis (GEPIA) database (http://gepia.cancer-pku.cn/) (16).

Statistical analysis

The gene expression profile data of the LUAD samples and the clinical information data were downloaded from TCGA database. The statistical analysis was performed using the GraphPad Prism (Version 9) and R packages. The student's *t*-test and paired t-test were used for the independent and paired groups, respectively. The results of the continuous variables are presented as the mean ± standard deviation. A P value ≤0.05 was considered statistically significant.

Results

STT3A is upregulated in LUAD and is correlated with a poor prognosis

Based on TCGA database, we initially identified 21 glycosyltransferases as DE among 535 LUAD patients, including STT3B, OGT, and STT3A (see *Figure 1A*). The Kaplan-Meier curves suggested that of the top 10 DE glycosyltransferases, only OGT and STT3A were related to the survival rate. Notably, OGT expression was inversely correlated with a poor prognosis, while STT3A expression was positively correlated with a poor prognosis (see Figure S1). We next analyzed the expression level of STT3A in the RNA-Seq data sets, and found that the level of STT3A was substantially increased in tumors (see *Figure 1B*). To further confirm the expression patterns of STT3A, we analyzed its expression levels in both human tissues and cell lines. The level of STT3A protein was significantly higher in tumor tissues than adjacent normal tissues (see *Figure 1C*). Combined with qRT-PCR and the IHC analysis, we confirmed that the STT3A levels were indeed increased in tumor tissues (see *Figures 1D,1E*). Additionally, STT3A was more elevated in lung cancer cell lines (H3122, H1975, H1299, HCC827, H292, H1650, A549, and PC-9) than normal human bronchial epithelial cell lines (BEAS-2B and MRC-5) (see *Figure 1F*). The patients acquired from TCGA and the GEO database (513 and 719 cases, respectively) with higher STT3A expression levels had a significantly worse OS rate than those with lower expression levels (log-rank test P=0.00033 and P=0.009, respectively; see *Figure 1G,1H*). Additionally, representative images of the different IHC staining intensity of STT3A in 183 TMA samples were scored, and the survival outcomes were similar; that is, higher STT3A expression

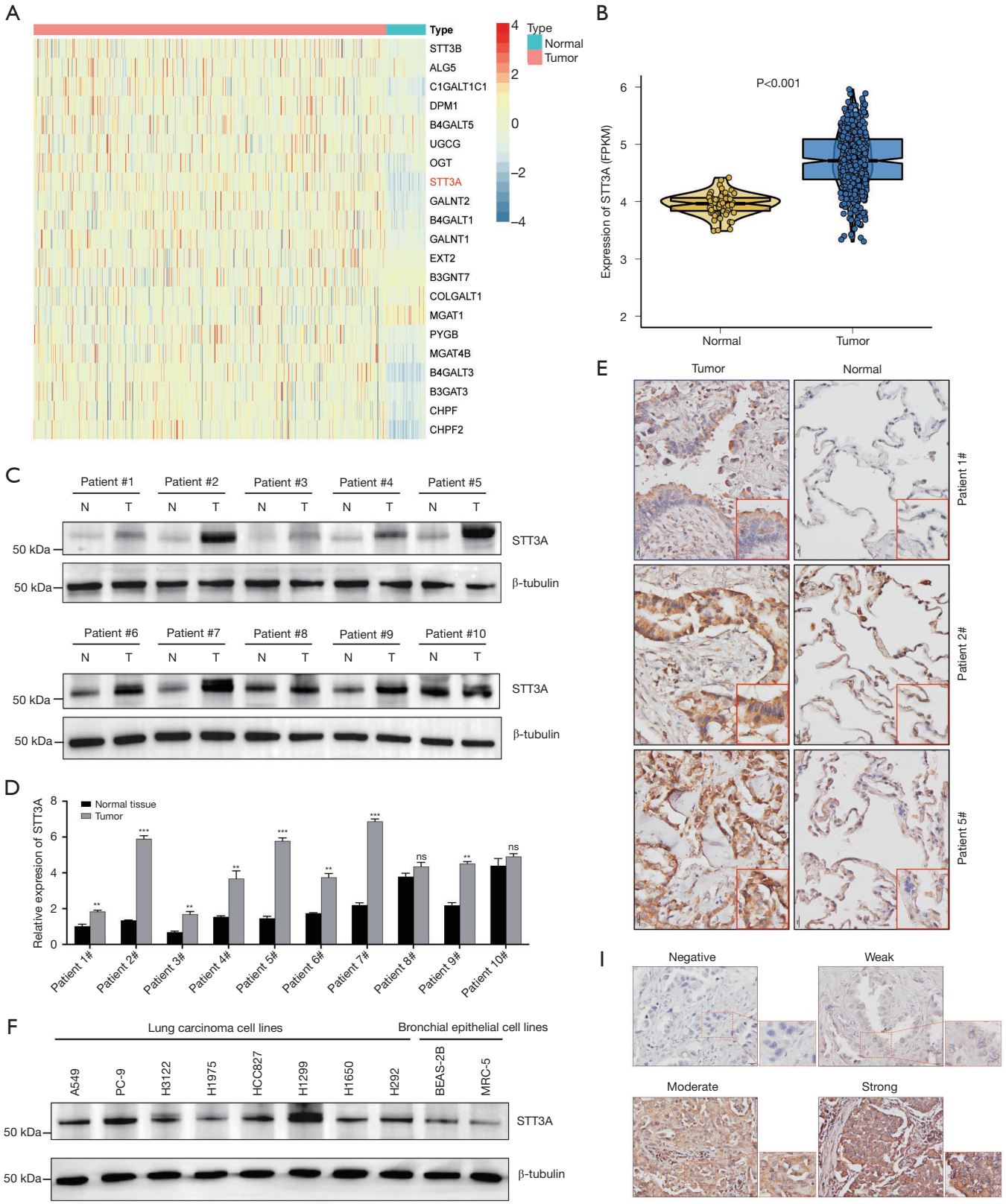

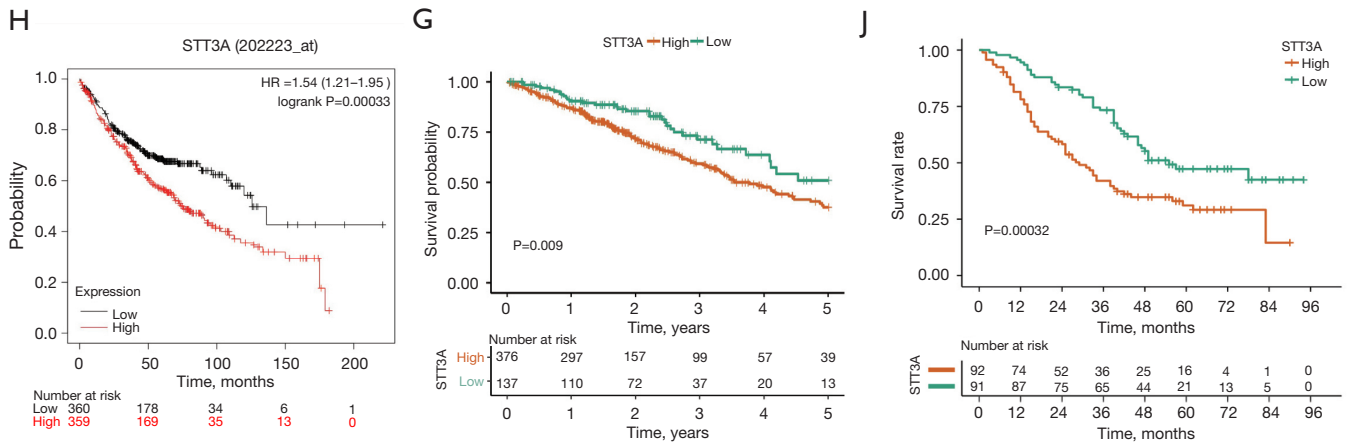

Figure 1 STT3A is highly expressed in lung cancer tissues and correlated with the poor prognosis of LUAD patients. (A) Heat map of DE glycosyltransferase in LUAD and normal adjacent tissues; (B) STT3A expression in TCGA database (normal: 59; tumor: 535); (C) Western blot analysis of the expression levels of STT3A in the tumor tissues and adjacent normal tissues of 10 clinical patients with LUAD; (D) the relative expression of STT3A in clinical specimens was detected by qRT-PCR (n=10); (E) IHC staining was performed in paired clinical specimens, and the results showed that STT3A was highly expressed in lung cancer tissues (scale bar: 20 μm); (F) the expression levels of STT3A in NSCLC cancerous cell lines, including H3122, H1975, H1299, HCC827, H292, H1650, A549, and PC-9 were examined by Western blot, and compared to normal human bronchial epithelial cell lines (BEAS-2B and MRC-5); (G) Kaplan-Meier analysis of OS according to TCGA database; the high expression of STT3A is correlated with a worse survival rate (P=0.009); (H) Kaplan-Meier analysis of OS according to the GEO cohort (P=0.00033); (I) representative images of different immunohistochemical staining intensities of STT3A in TMA. Scale bar: 20 μm. (J) High STT3A expression was associated with poor OS in LUAD patients in the TMA samples. **, P<0.01; ***, P<0.001; ns, not significant. STT3A, STT3 oligosaccharyltransferase complex catalytic subunit A; LUAD, lung adenocarcinoma; TCGA, The Cancer Genome Atlas; qRT-PCR, quantitative real-time polymerase chain reaction; IHC, immunochemistry; NSCLC, non-small cell lung cancer; OS, overall survival; GEO, Gene Expression Omnibus; TMA, tissue microarray.

levels were associated with a poor prognosis (log-rank test, P=0.00032; see *Figure 1I,1J*). The correlation analysis between different IHC staining intensity of STT3A and clinicopathological factors showed that only the lymph node status and metastasis were marginally significant (chi-square test, P=0.0893, P=0.0791; see Table S1).

Knockout of STT3A inhibits tumor cell proliferation and colony formation by inducing cell-cycle arrest

To examine the functional role of STT3A in tumor cells, an in-depth analysis was conducted in relation to proliferation, colony formation, and the cell-cycle checkpoint. CRISPR/Cas9-mediated STT3A knockout was performed in 2 highly expressed cell lines (PC-9 and H1299), and the knockout efficiencies were verified by Western blotting (see *Figure 2A*). As expected, cell proliferation was significantly repressed in STT3A knockout cells, and colony formation ability was also more decreased in both the PC-9-sgSTT3A and H1299-sgSTT3A cells than the negative control cells (see *Figure 2B,2C*). Flow cytometry analysis showed no significant changes in cell apoptosis (see *Figure 2D*). Further, accumulated G0/G1 phase cell population was examined in the knockout cells. The decreased S-phase cell population suggested cell-cycle arrest at G1/S transition (see *Figure 2E,2F*). As the key mediators for the G0/G1 cell-cycle checkpoint, the expression levels of CDK4 and CDK6 were downregulated and the p27 protein was upregulated in the STT3A depleted cells. However, no significant upregulation of the p21 protein was detected in PC-9-sgSTT3A and H1299-sgSTT3A cells (see *Figure 2G*). Together, these results indicate that STT3A knockout had an inhibitory effect on tumor cell proliferation by upregulating p27 and downregulating CDK4 and CDK6.

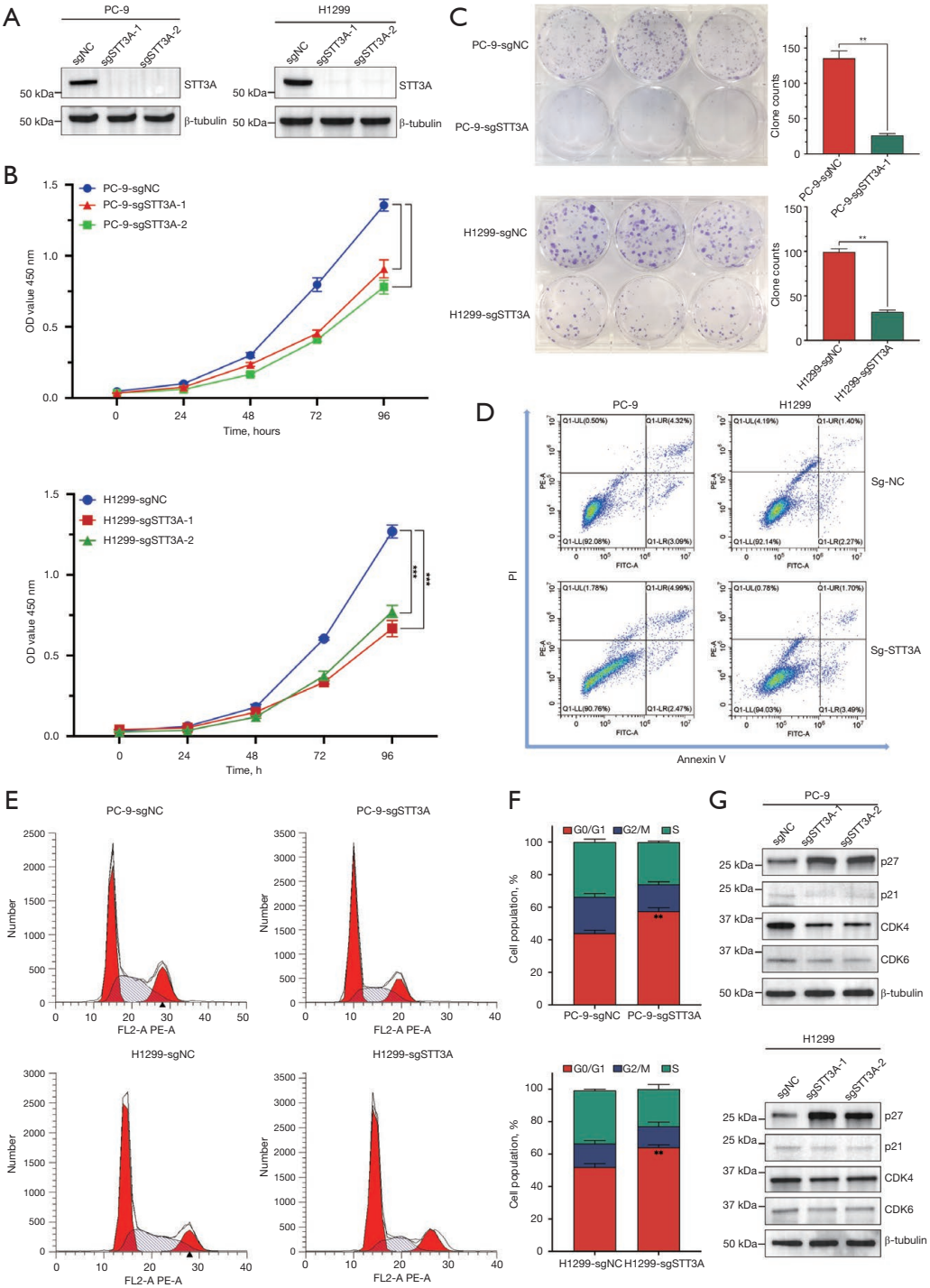

Figure 2 STT3A knockout inhibits tumor cell growth. (A) Establishment of STT3A knockout cell lines in PC-9 and H1299 verified by Western blot. (B) STT3A knockout significantly inhibited PC-9 and H1299 cell proliferation. (C, D) STT3A knockout also significantly affected the colony formation ability of these cell lines but did not lead to apoptosis. (E) Effect of STT3A knockout on the G0/G1 cell-cycle transition was detected in the PC-9 and H1299 cells by PI staining and flow cytometry. (F) The quantification data was analyzed by ModFit 5. (G) STT3A regulated the expression of the cell-cycle transition mediators, including CDK4, CDK6, p21, and p27. Staining method for (C): 0.1% crystal violet. The data are presented as mean ± standard deviation according to the Student's *t*-test. **, P<0.01; ***, P<0.001. sgNC, small guide RNA negative control; sgSTT3A, small guide RNA of STT3A; STT3A, STT3 oligosaccharyltransferase complex catalytic subunit A; PI, propidium iodide.

STT3A regulates tumor cell invasion and migration by activating EMT signaling

To determine whether STT3A modulates tumor cell invasion and migration, we subsequently used transwell chamber assays in the PC-9 and H1299 cells. The transwell results showed that the depletion of STT3A significantly suppressed tumor cell migration ability (see *Figure 3A*). Similarly, the number of invasive cells was statistically decreased in the knockout groups compared to the controls (see *Figure 3B*). Additionally, the wound-healing assay revealed reduced migration ability according to the width of the wound after 24 and 48 h (see *Figure 3C,3D*). Based on the outcomes, we hypothesized that STT3A regulated cell functions via EMT signaling, and thus we evaluated the essential marker genes for EMT. Consistent with our predictions, E-cadherin was considerably elevated while N-cadherin and vimentin were decreased in STT3A knockout cell lines (see *Figure 3E*). These results provide further evidence that STT3A suppresses migration and invasion targeting EMT.

Suppression of STT3A by the small compound NGI-1 reduces tumor proliferation, migration, and invasion

NGI-1 is a small-molecule inhibitor that partially represses N-glycosylation by targeting the active catalytic subunits of OST complexes, the STT3A, and STT3B. The CCK-8 assays revealed that cell proliferation was more inhibited in the PC-9 and H1299 tumor cells following the NGI-1 treatment than the DMSO controls (see *Figure 4A*). Notably, cell apoptosis was not enhanced in both cell lines, but cell-cycle transition was affected by an accumulation of the cell population in the G0/G1 phase and a reduction in the S phase (see *Figure 4B,4C*). Similar outcomes were observed in the transwell and wound-healing assays, which showed a decrease of migration and invasion abilities in tumor cells treated with NGI-1 inhibitors (see *Figure 4D-4F*).

STT3A affects the activation of AKT and MAPK signaling by mediating EGFR glycosylation

Intrigued by the above findings, we then sought to reveal the potential mechanism by which STT3A suppresses the cell cycle and EMT using 4D label-free quantitative proteomics. In total, we identified 1,194 upregulated and 1,121 downregulated proteins as DE in 3 paired cell samples (PC-9-sgSTT3A *vs.* PC-9-sgNC; q value <0.05 and FC >1.5; see *Figure 5A*). *Figure 5B,5C* show a heat map and hierarchical clustering of the top 40 significantly DE proteins. Among them, 236 membrane proteins were downregulated, including the EGFR, CTK39 and β-arrestin1 (ARRB1) proteins (see *Figure 5D* and Figure S2A).

The most abundant gene ontology (GO) terms for the BPs were allocated to the cellular process, biological regulation, and metabolic process, while the Cluster of Orthologous Groups (COG) analysis was mainly enriched in PTMs, signaling transduction mechanisms, and cell-cycle control (see *Figures 5E,5F*, and Figure S2B-S2D). The Kyoto Encyclopedia of Genes and Genomes (KEGG) analysis revealed that the non-small cell lung cancer and mitogen-activated protein kinase (MAPK) signaling pathways were mainly enriched, which was further confirmed by Western blot assays examining marker proteins (see *Figure 5G*). As a result, EGFR and p-EGFR expression were dramatically decreased, while the downstream targeted proteins AKT, MEK, and ERK showed no changes. Additionally, the expression levels of p-AKT, p-MEK, and p-ERK were also reduced, which strongly suggested that the phosphorylation process was significantly suppressed by STT3A deletion, leading to the inactivation of the AKT and MAPK signaling pathway (see *Figure 5H*). Similar evidence was found in NGI-1 treated cells in which the phosphorylation of the AKT and MAPK signaling pathway was restrained (see *Figure 5I*). Taken together, these results show that the knockout or suppression of STT3A abrogated the effects of protein glycosylation, thereby inhibiting the downstream AKT and MAPK signaling pathways.

Knockout of STT3A inhibits LUAD tumor growth in xenografts

To confirm the inhibitory effects on lung cancer growth of STT3A depletion, we established xenograft tumor formation mice models with prepared PC-9-sgNC and PC-9-sgSTT3A cell lines. The tumor cells were inoculated subcutaneously in the nude mice, and 20 mice were then sacrificed 5 weeks after injection for *in-vivo* experiments. In accordance with the *in-vitro* experimental results, a significant reduction in tumor growth and tumor sizes was observed on the side implanted with the PC-9-sgSTT3A cell lines (see *Figure 6A-6D*). Moreover, IHC analysis showed that Ki67, EGFR and STT3A expression was decreased in knockout mice (see *Figure 6E*). To further

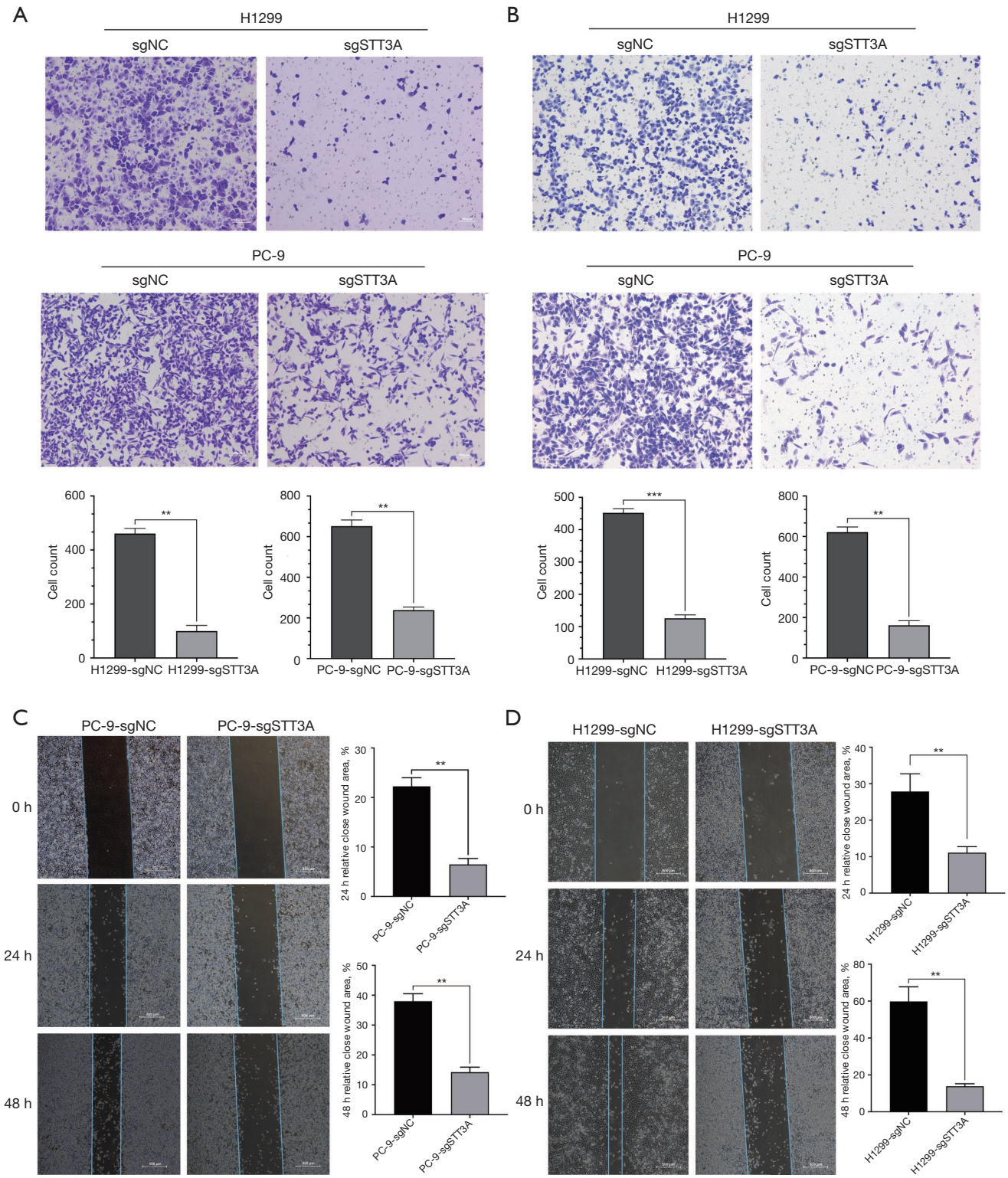

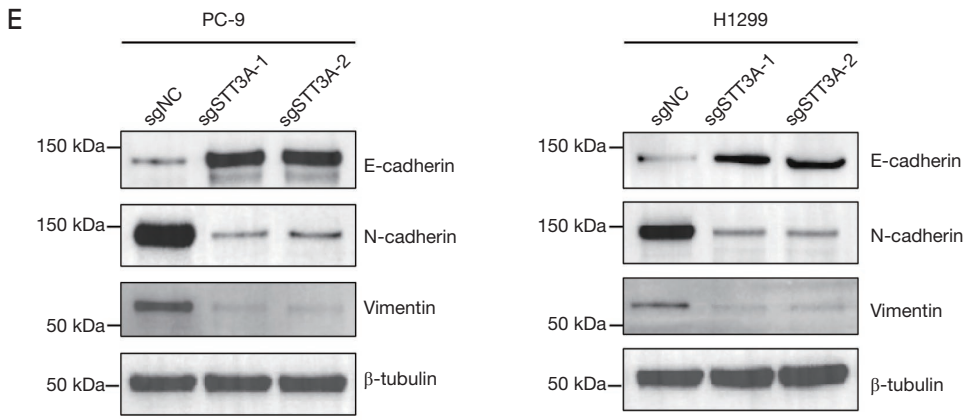

Figure 3 STT3A knockout inhibits tumor invasion and migration via EMT. (A) Knockout of STT3A inhibited PC-9 and H1299 cell migration detected by transwell assays: cell counts for the transwell assays are indicated below. Scale bar: 100 μm. (B) Transwell assays with Matrigel were used to confirm the effects of STT3A on tumor cell invasiveness. Scale bar: 100 μm. (C,D) The migration ability of the transfected PC-9 and H1299 cells was verified by a wound-healing experiment. The quantification data are also indicated, Scale bar: 500 μm. (E) Western blot analysis of EMT-related proteins E-cadherin, N-cadherin, vimentin. Staining method for (A,B): 0.1% crystal violet; magnification, ×100. The data are presented as mean ± standard deviation according to the Student's *t*-test. **, P<0.01; ***, P<0.001. sgNC, small guide RNA negative control; sgSTT3A, small guide RNA of STT3A; STT3A, STT3 oligosaccharyltransferase complex catalytic subunit A; EMT, epithelial-mesenchymal transition.

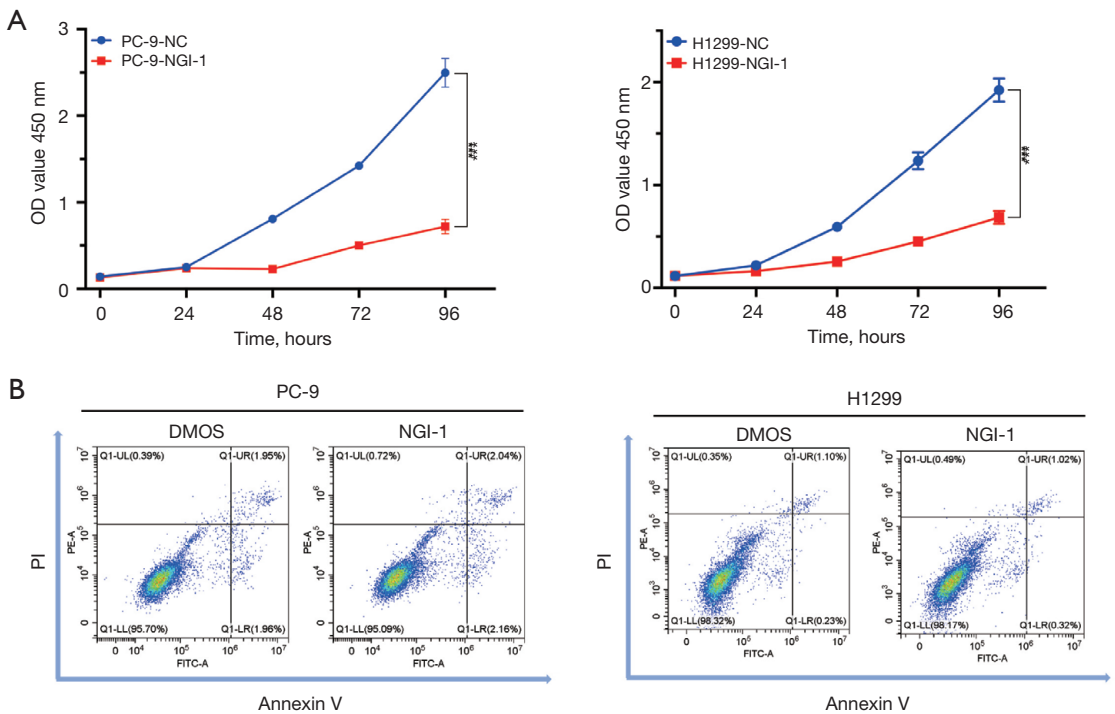

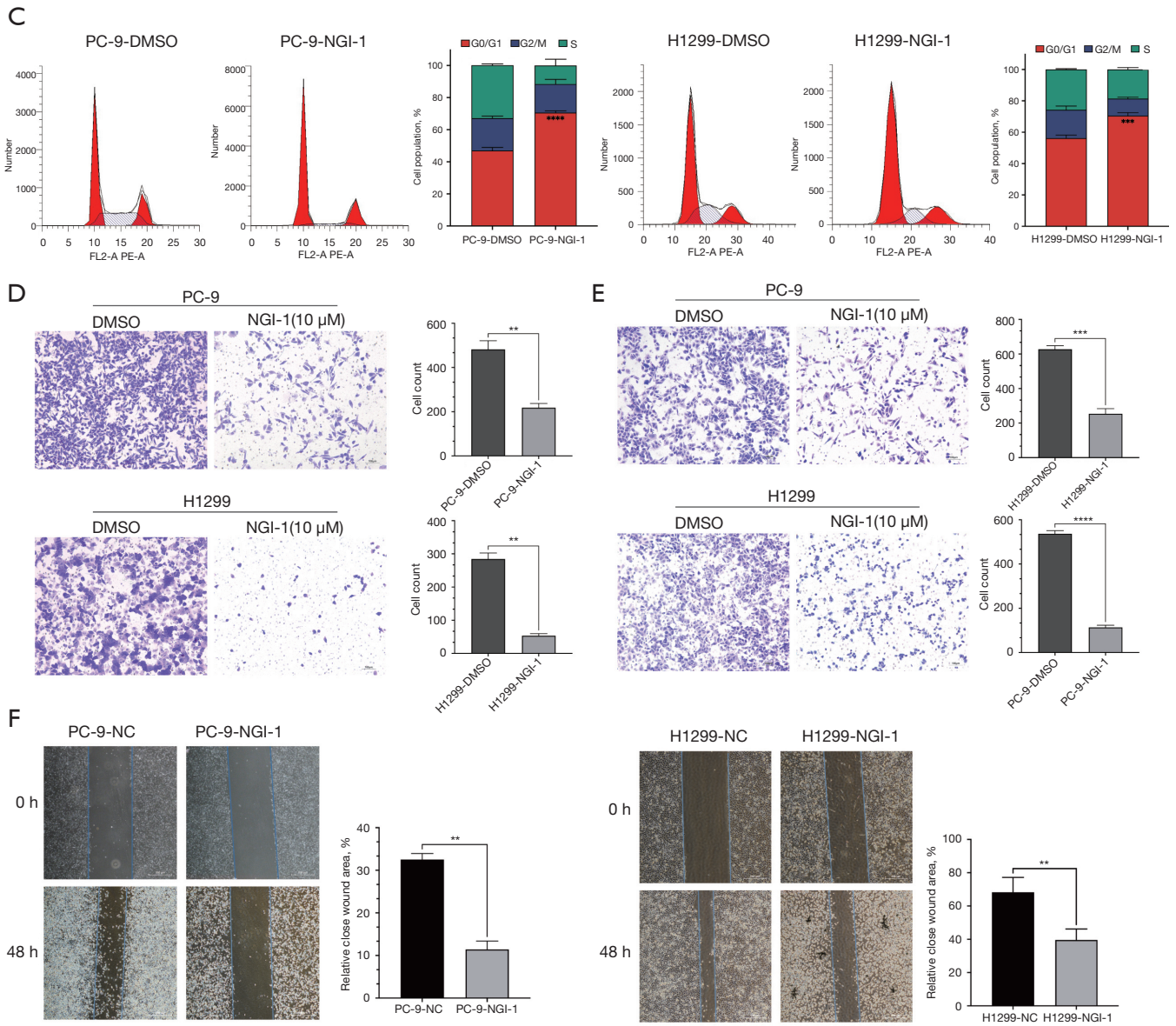

Figure 4 The STT3A inhibitor NGI-1 confirmed its effect on the biological behavior of lung adenocarcinoma cells. (A,B) NGI-1 inhibited PC-9 and H1299 cell proliferation, without inducing apoptosis in both cell lines. (C) Consistent with the knockout group, NGI-1 significantly affected the G0/G1 cell-cycle transition, and the quantification data were analyzed by ModFit 5. (D,E) The migration and invasion ability of NGI-1 treated cells was evaluated by Transwell assay (with or without Matrigel). Scale bar: 100 μm. (F) The wound-healing experiment also confirmed the effect of the STT3A inhibitor on cell migration ability, Scale bar: 500 μm. The histograms are based on the quantification data for the reciprocal assays in (D-F). PI, Propidium Iodide. Staining method for (D,E): 0.5% crystal violet; magnification, ×100. The data are presented as the mean ± standard deviation according to the Student's *t*-test. **, P<0.01; ***, P<0.001, ****, P<0.0001. STT3A, STT3 oligosaccharyltransferase complex catalytic subunit A.

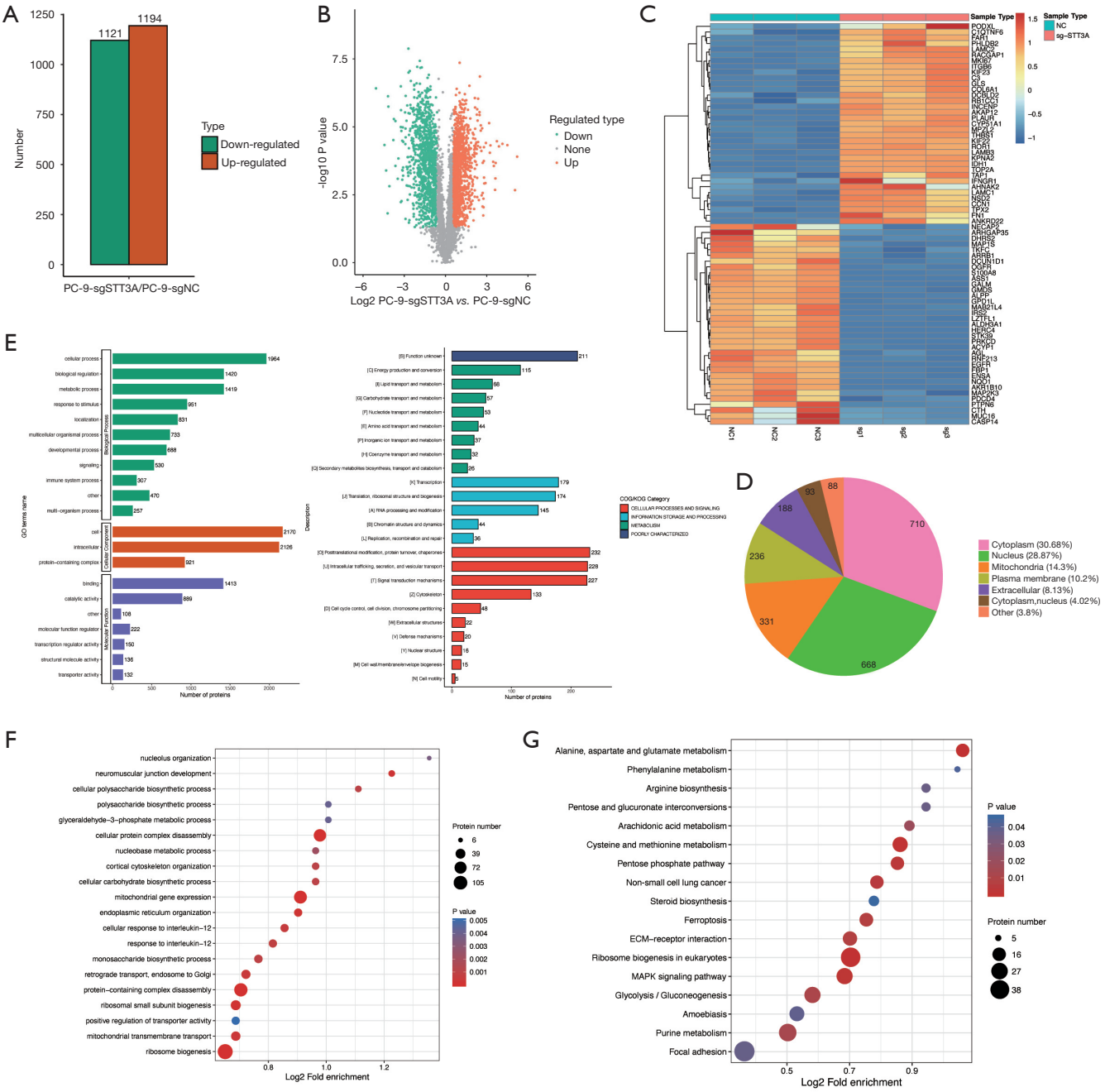

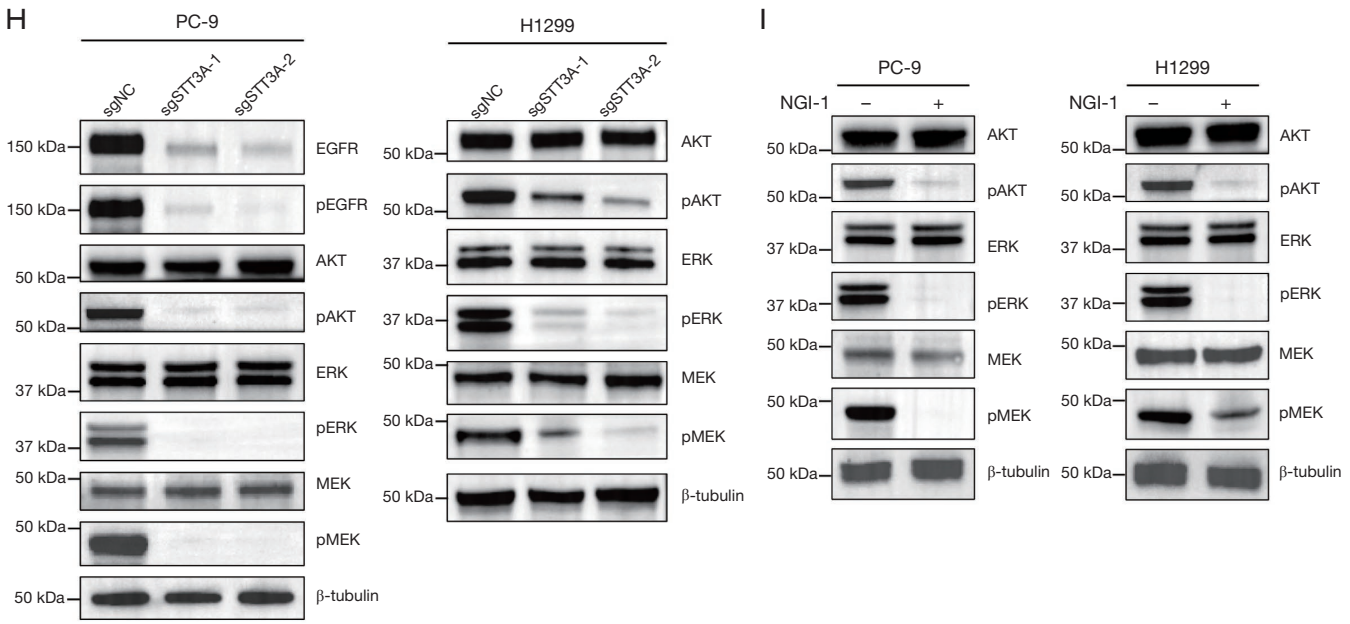

Figure 5 The proteomic changes of PC-9 after STT3A knockout were detected by MS. We confirmed that STT3A regulates tumors through the Akt and MAPK signaling pathways. (A) The protein levels of 3 pairs of PC-9-sgSTT3A and PC-9-sgNC were detected by 4D-label-free quantitative proteomics. Using 1/1.5 as the threshold of change, 1,121 proteins were significantly downregulated and 1,194 were significantly upregulated. (B) A volcano map of changing proteins. (C) EGFR, CTK39, ARRB1 and other key proteins were downregulated in the top 40 heat maps of the changing proteins. (D) Among them, 236 membrane proteins were significantly different. (E) GO enrichment analysis revealed changes in BP, cellular component, and molecular function, and the COG analysis revealed changes in cell cycle and cell signaling pathway. (F) The changes of the GO analysis in BPs were mainly concentrated in the cellular process, biological regulation, and mitochondrial metabolism. (G) The KEGG pathway enrichment analysis showed that changes in STT3A knockout signaling pathways were enriched in NSCLC and the MAPK signaling pathways; the NSCLC signaling pathway included the AKT signaling pathway. (H) Total and phosphorylated forms of AKT, MEK, and ERK proteins were examined by immunoblot with indicated antibodies in transfected cell lines. (I) The inhibition of AKT and MAPK signals after STT3A inhibitor treatment was confirmed by Western blot; +, means cells were treated with NGI-1 (10 μM); –, means cells were treated with DMSO of the same volume as NGI-1. STT3A, STT3 oligosaccharyltransferase complex catalytic subunit A; MS, mass spectrometry; MAPK, mitogen-activated protein kinase; GO, Gene Ontology; BP, biological process; COG, Cluster of Orthologous Groups; KEGG, Kyoto Encyclopedia of Genes and Genomes; NSCLC, non-small cell lung cancer; AKT, protein kinase B; MEK, mitogen-activated protein kinase kinase 1/2; ERK, extracellular regulated protein kinases 1/2.

examine the inhibitory effects on tumor proliferation, 14 nude mice were randomly divided into 2 groups and then received the NGI-1 treatment (see *Figure 6F*). Compared with the placebo group, the PC-9 tumor xenografts grew significantly slower after the NGI-1 treatment. Additionally, the tumor volumes and wet weight in NGI-1 treated mice were significantly smaller at the end point than those of the DMSO controls (see *Figure 6G-6I*).

Discussion

Glycosylation is one of the most important post-PTMs for maintaining stability and the subcellular localization of proteins (19,20). The aberrant glycosylation of critical proteins has been demonstrated to be involved in the tumorigenesis, development, metastasis, and tumor microenvironment regulation of multiple cancers (10,21). STT3A is a major catalytic subunit of OST and plays a key role in the N-glycosylation of proteins (22). However, the relationship between STT3A and cancer is still poorly understood (15). For the first time, we systematically analyzed the expression, prognostic value, and functions of STT3A in LUAD. Based on TCGA and the GEO data sets and the clinical LUAD tissues, we found that STT3A was frequently overexpressed in the LUAD tissues than the normal lung tissues, and the high expression of

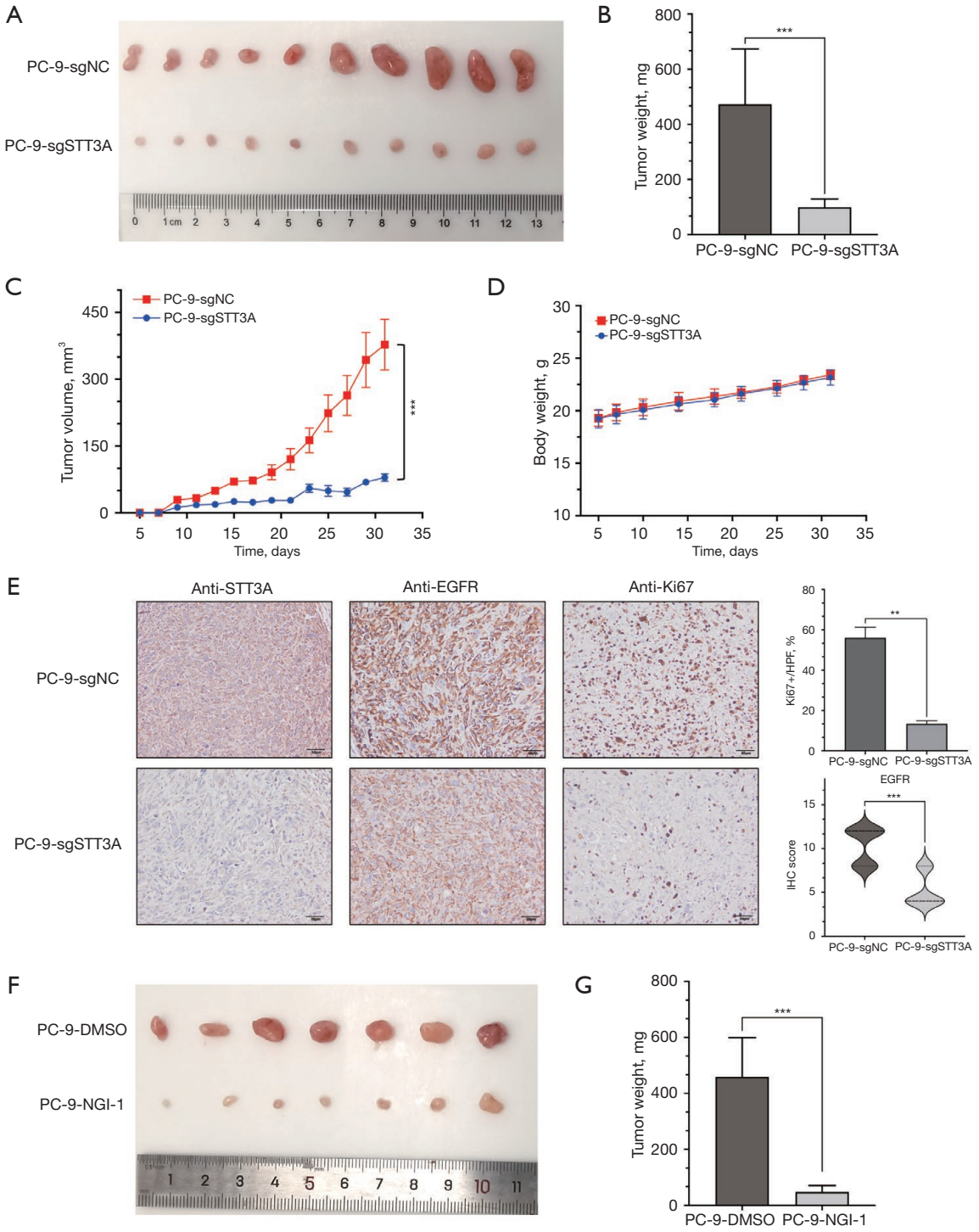

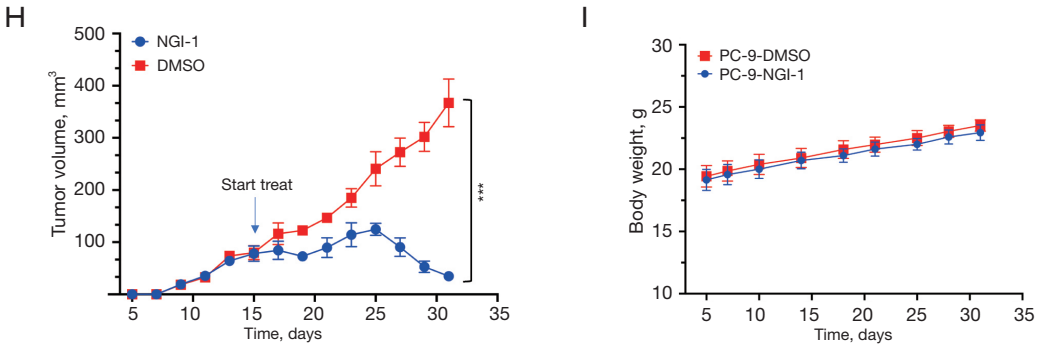

Figure 6 The effect of STT3A inhibition on the progression of LUAD was verified *in vivo*. (A-C) STT3A knockout inhibited xenograft tumor formation *in vivo*. Representative xenograft tumor images (A), tumor weight (B), tumor volume (C) and body weight (D). (E) Representative IHC staining of STT3A, EGFR, and Ki67 for indicated xenograft tumors. Quantification data were also indicated. Scale bar: 50 μm. Mice were treated with the STT3A inhibitor NGI-1 and compared to a placebo group (7 mice for each group). (F-I) NGI-1 inhibited xenograft tumor formation *in vivo*. Representative xenograft tumor images (F), tumor weight (G), tumor volume (H) and body weight (I). The data are presented as the mean ± standard deviation according to the Student's *t*-test. **, P<0.01; ***, P<0.001. LUAD, lung adenocarcinoma; sgNC, small guide RNA negative control; sgSTT3A, small guide RNA of STT3A; IHC, immunohistochemistry.

STT3A was significantly associated with the poor OS of LUAD patients. Further, our *in-vitro* experiments showed that the knockout or inhibition of STT3A suppressed the proliferation, migration, and invasion of LUAD cells by arresting the cell cycle and EMT. Similarly, the knockout or inhibition of STT3A robustly suppressed tumor growth in xenograft tumor models. These findings suggest that STT3A promotes LUAD progression and could serve as a novel prognostic marker and potential therapeutic target for LUAD patients.

As a key glycosyltransferase, STT3A may catalyze the N-glycosylation of various proteins and thus affect their biological and physiological functions. To explore the underlying mechanisms and signaling pathways of STT3A in promoting LUAD progression, we also performed a quantitative proteomic analysis and found that 1,121 proteins were significantly more upregulated and 1,194 proteins were significantly more downregulated in the STT3A-knockout cells than the control cells. Thousands of DE proteins indicated that there was a complex molecular network downstream of STT3A. Indeed, the KEGG pathway analysis revealed that these DE proteins were significantly enriched in various cancer-related pathways, including the canonical MAPK and phosphatidylinositol-3-kinase and protein kinase B (PI3K/AKT) signaling pathways, which are critical for cell growth and survival. In subsequent validation experiments, we found that the phosphorylation of MEK, ERK, and AKT were robustly reduced in the STT3A-knockout cell lines, and further confirmed the effect of STT3A on the activation of the MAPK and PI3K/AKT pathways. Collectively, these findings provide direct evidence that the ability of STT3A to promote LUAD progression depends, at least partially, on the downstream activation of the MAPK and PI3K/AKT signaling pathways.

EMT is an essential process for cancer initiation and progression (23). The epithelial-mesenchymal phenotypic conversion allows cancer cells to acquire enhanced capacities of invasion and metastasis (24). In this study, we also investigated whether STT3A affected the EMT of LUAD cells. We found that the knockout of STT3A led to the reduced expression of mesenchymal markers (N-cadherin and vimentin). Conversely, the expression of E-cadherin, the epithelial marker, was increased following the knockout of STT3A. Similarly, the invasiveness of STT3A-knockout cells was significantly suppressed compared to that of controls. Thus, our study indicates that the regulation of EMT is another function of STT3A that promotes LUAD progression.

It is well known that EFGR is a key driver of multiple malignancies, including LUAD. The hyperactivation or overexpression of EGFR can induce tumorigenesis and cancer progression by activating the downstream RAS/MAPK, PI3K/AKT, and JAK/STAT signaling pathways (25). EGFR has also been identified as a driver of EMT (26,27). N-linked glycosylation plays critical role in maintaining the structure and stability of EGFR (28). Previous studies have shown that NGI-1, a N-link glycosylation inhibitor

that targets both the STT3A and STT3B subsets of OST, inhibits the activation of the EGFR signaling pathways by blocking EGFR glycosylation (29,30). In the present study, we found that the knockout of STT3A downregulated EGFR expression and inhibited EGFR activation in the PC-9 cell line harboring the *EGFR* 19 exon deletion. Based on the canonical function of STT3A, these results are probably due to the de-glycosylation and degradation of the EGFR protein after STT3A deletion.

In addition to EGFR, other proteins, such as ARRB1, S100 calcium-binding protein A8 (S100A8), and serine/threonine kinase 39 (STK39), may also be involved in the STT3A-induced MAPK, PI3K/ERK, and EMT pathway activation. ARRB1 has been shown to be an activator of the AKT and ERK signaling pathways and to accelerate the cell-cycle progression and cell proliferation of multiple cancers (31-33). The function of STK39 in promoting the progression of cholangiocarcinoma by activating the PI3K/AKT signaling pathway has also been reported (34). S100A8 is a regulator of the EMT and AKT pathways and has been shown to promote migration, invasion, and metastasis in multiple cancers (35-37). All these proteins were significantly downregulated by the knockout of STT3A based on the results of the quantitative proteomic analysis in our study, indicating that they are potential target of STT3A. Additionally, these proteins may help explain how STT3A regulates the above-mentioned signaling pathways in the H1299 cell line not driven by EGFR. However, the interaction and regulating mechanisms between STT3A and these 3 proteins require further investigation.

Conclusions

In summary, we examined the molecular function of STT3A and its potential underlying regulatory mechanism in LUAD in both clinical samples and cell lines. Based on the bioinformatics analysis and biological experiments, we demonstrated that the knockout and suppression of STT3A has inhibitory effects on cell proliferation and invasion and that this regulatory event is accomplished via AKT-MAPK signaling. Thus, targeting STT3A represents a promising therapeutic strategy and extends understandings of lung cancer progression.

Acknowledgments

The authors appreciate the academic support from the AME Lung Cancer Collaborative Group.
Funding: This research was funded by the National Natural Science Foundation of China (No. 31771549 to Y Chen) and Key Projects of Sichuan Province (No. 2021YFS0233 and No. 2021-YF05-00751-SN to J Cheng). This work was also supported by the 1.3.5 Project for Disciplines of Excellence, West China Hospital, Sichuan University (No. ZYGD18021 to L Liu).

Footnote

Reporting Checklist: The authors have completed the ARRIVE reporting checklist. Available at https://tlcr.amegroups.com/article/view/10.21037/tlcr-22-396/rc

Data Sharing Statement: Available at https://tlcr.amegroups.com/article/view/10.21037/tlcr-22-396/dss

Conflicts of Interest: All authors have completed the ICMJE uniform disclosure form (available at https://tlcr.amegroups.com/article/view/10.21037/tlcr-22-396/coif). The authors have no conflicts of interest to declare.

Ethical Statement: The authors are accountable for all aspects of the work in ensuring that questions related to the accuracy or integrity of any part of the work are appropriately investigated and resolved. The study was conducted in accordance with the Declaration of Helsinki (as revised in 2013). The study was approved by the Ethics Committee of the West China Hospital, Sichuan University (No. 2021-1746). Informed consent of patients was waived for this study after the approval of the ethics committee. Animal experiments *in vivo* were approved by the Animal Ethics Committee of the West China Hospital, Sichuan University (No. 2021987A), in compliance with institutional guidelines for the care and use of animals

References

1. Siegel RL, Miller KD, Fuchs HE, et al. Cancer Statistics, 2021. CA Cancer J Clin 2021;71:7-33.
2. Howlader N, Forjaz G, Mooradian MJ, et al. The Effect of Advances in Lung-Cancer Treatment on Population Mortality. N Engl J Med 2020;383:640-9.
3. Oliveira-Ferrer L, Legler K, Milde-Langosch K. Role of protein glycosylation in cancer metastasis. Semin Cancer Biol 2017;44:141-52.
4. Saito T, Miyoshi E, Sasai K, et al. A secreted type of beta 1,6-N-acetylglucosaminyltransferase V (GnT-V) induces tumor angiogenesis without mediation of glycosylation: a novel function of GnT-V distinct from the original glycosyltransferase activity. J Biol Chem 2002;277:17002-8.
5. Ihara S, Miyoshi E, Ko JH, et al. Prometastatic effect of N-acetylglucosaminyltransferase V is due to modification and stabilization of active matriptase by adding beta 1-6 GlcNAc branching. J Biol Chem 2002;277:16960-7.
6. Zhang Y, Fan C, Zhang L, et al. Glycosylation-dependent antitumor therapeutic monoclonal antibodies. Prog Mol Biol Transl Sci 2019;163:471-85.
7. Murata K, Miyoshi E, Kameyama M, et al. Expression of N-acetylglucosaminyltransferase V in colorectal cancer correlates with metastasis and poor prognosis. Clin Cancer Res 2000;6:1772-7.
8. Takahashi T, Hagisawa S, Yoshikawa K, et al. Predictive value of N-acetylglucosaminyltransferase-V for superficial bladder cancer recurrence. J Urol 2006;175:90-3; discussion 93.
9. Reily C, Stewart TJ, Renfrow MB, et al. Glycosylation in health and disease. Nat Rev Nephrol 2019;15:346-66.
10. Pinho SS, Reis CA. Glycosylation in cancer: mechanisms and clinical implications. Nat Rev Cancer 2015;15:540-55.
11. Mohanty S, Chaudhary BP, Zoetewey D. Structural Insight into the Mechanism of N-Linked Glycosylation by Oligosaccharyltransferase. Biomolecules 2020;10:624.
12. Wild R, Kowal J, Eyring J, et al. Structure of the yeast oligosaccharyltransferase complex gives insight into eukaryotic N-glycosylation. Science 2018;359:545-50.
13. Ruiz-Canada C, Kelleher DJ, Gilmore R. Cotranslational and posttranslational N-glycosylation of polypeptides by distinct mammalian OST isoforms. Cell 2009;136:272-83.
14. Hsu JM, Xia W, Hsu YH, et al. STT3-dependent PD-L1 accumulation on cancer stem cells promotes immune evasion. Nat Commun 2018;9:1908.
15. Chan LC, Li CW, Xia W, et al. IL-6/JAK1 pathway drives PD-L1 Y112 phosphorylation to promote cancer immune evasion. J Clin Invest 2019;129:3324-38.
16. Tang Z, Li C, Kang B, et al. GEPIA: a web server for cancer and normal gene expression profiling and interactive analyses. Nucleic Acids Res 2017;45:W98-W102.
17. Carrot-Zhang J, Chambwe N, Damrauer JS, et al. Comprehensive Analysis of Genetic Ancestry and Its Molecular Correlates in Cancer. Cancer Cell 2020;37:639-654.e6.
18. Győrffy B, Surowiak P, Budczies J, et al. Online survival analysis software to assess the prognostic value of biomarkers using transcriptomic data in non-small-cell lung cancer. PLoS One 2013;8:e82241.
19. Xu C, Ng DT. Glycosylation-directed quality control of protein folding. Nat Rev Mol Cell Biol 2015;16:742-52.
20. Freeze HH, Ng BG. Golgi glycosylation and human inherited diseases. Cold Spring Harb Perspect Biol 2011;3:a005371.
21. Xu Y, Wang Y, Höti N, et al. The next "sweet" spot for pancreatic ductal adenocarcinoma: Glycoprotein for early detection. Mass Spectrom Rev 2021. [Epub ahead of print].
22. Braunger K, Pfeffer S, Shrimal S, et al. Structural basis for coupling protein transport and N-glycosylation at the mammalian endoplasmic reticulum. Science 2018;360:215-9.
23. Bakir B, Chiarella AM, Pitarresi JR, et al. EMT, MET, Plasticity, and Tumor Metastasis. Trends Cell Biol 2020;30:764-76.
24. Singh M, Yelle N, Venugopal C, et al. EMT: Mechanisms and therapeutic implications. Pharmacol Ther 2018;182:80-94.
25. da Cunha Santos G, Shepherd FA, Tsao MS. EGFR mutations and lung cancer. Annu Rev Pathol 2011;6:49-69.
26. Zuo JH, Zhu W, Li MY, et al. Activation of EGFR promotes squamous carcinoma SCC10A cell migration and invasion via inducing EMT-like phenotype change and MMP-9-mediated degradation of E-cadherin. J Cell Biochem 2011;112:2508-17.
27. Voon DC, Wang H, Koo JK, et al. EMT-induced stemness and tumorigenicity are fueled by the EGFR/Ras pathway. PLoS One 2013;8:e70427.
28. Liao C, An J, Tan Z, et al. Changes in Protein Glycosylation in Head and Neck Squamous Cell Carcinoma. J Cancer 2021;12:1455-66.
29. Lopez-Sambrooks C, Shrimal S, Khodier C, et al. Oligosaccharyltransferase inhibition induces senescence in RTK-driven tumor cells. Nat Chem Biol 2016;12:1023-30.

30. Lopez Sambrooks C, Baro M, Quijano A, et al. Oligosaccharyltransferase Inhibition Overcomes Therapeutic Resistance to EGFR Tyrosine Kinase Inhibitors. Cancer Res 2018;78:5094-106.
31. Zhang YX, Li XF, Yuan GQ, et al. β-Arrestin 1 has an essential role in neurokinin-1 receptor-mediated glioblastoma cell proliferation and G2/M phase transition. J Biol Chem 2017;292:8933-47.
32. Zhang Z, Zhong X, Xiao Y, et al. MicroRNA-296 inhibits colorectal cancer cell growth and enhances apoptosis by targeting ARRB1-mediated AKT activation. Oncol Rep 2019;41:619-29.
33. Yang Y, Guo Y, Tan S, et al. β-Arrestin1 enhances hepatocellular carcinogenesis through inflammation-mediated Akt signalling. Nat Commun 2015;6:7369.
34. Hao X, Zhang Y, Lu Y, et al. STK39 enhances the progression of Cholangiocarcinoma via PI3K/AKT pathway. iScience 2021;24:103223.
35. Yin C, Li H, Zhang B, et al. RAGE-binding S100A8/A9 promotes the migration and invasion of human breast cancer cells through actin polymerization and epithelial-mesenchymal transition. Breast Cancer Res Treat 2013;142:297-309.
36. Tanigawa K, Tsukamoto S, Koma YI, et al. S100A8/A9 Induced by Interaction with Macrophages in Esophageal Squamous Cell Carcinoma Promotes the Migration and Invasion of Cancer Cells via Akt and p38 MAPK Pathways. Am J Pathol 2022;192:536-52.
37. Li S, Zhang J, Qian S, et al. S100A8 promotes epithelial-mesenchymal transition and metastasis under TGF-β/USF2 axis in colorectal cancer. Cancer Commun (Lond) 2021;41:154-70.

(English Language Editor: L. Huleatt)

Cite this article as: Cheng J, Xia L, Hao X, Gan F, Bai Y, Zhang C, Mao Y, Zhu Y, Pu Q, Park DW, Tavolari S, Mei J, Chen Y, Deng S, Liu L. Targeting STT3A produces an anti-tumor effect in lung adenocarcinoma by blocking the MAPK and PI3K/AKT signaling pathway. Transl Lung Cancer Res 2022;11(6):1089-1107. doi: 10.21037/tlcr-22-396

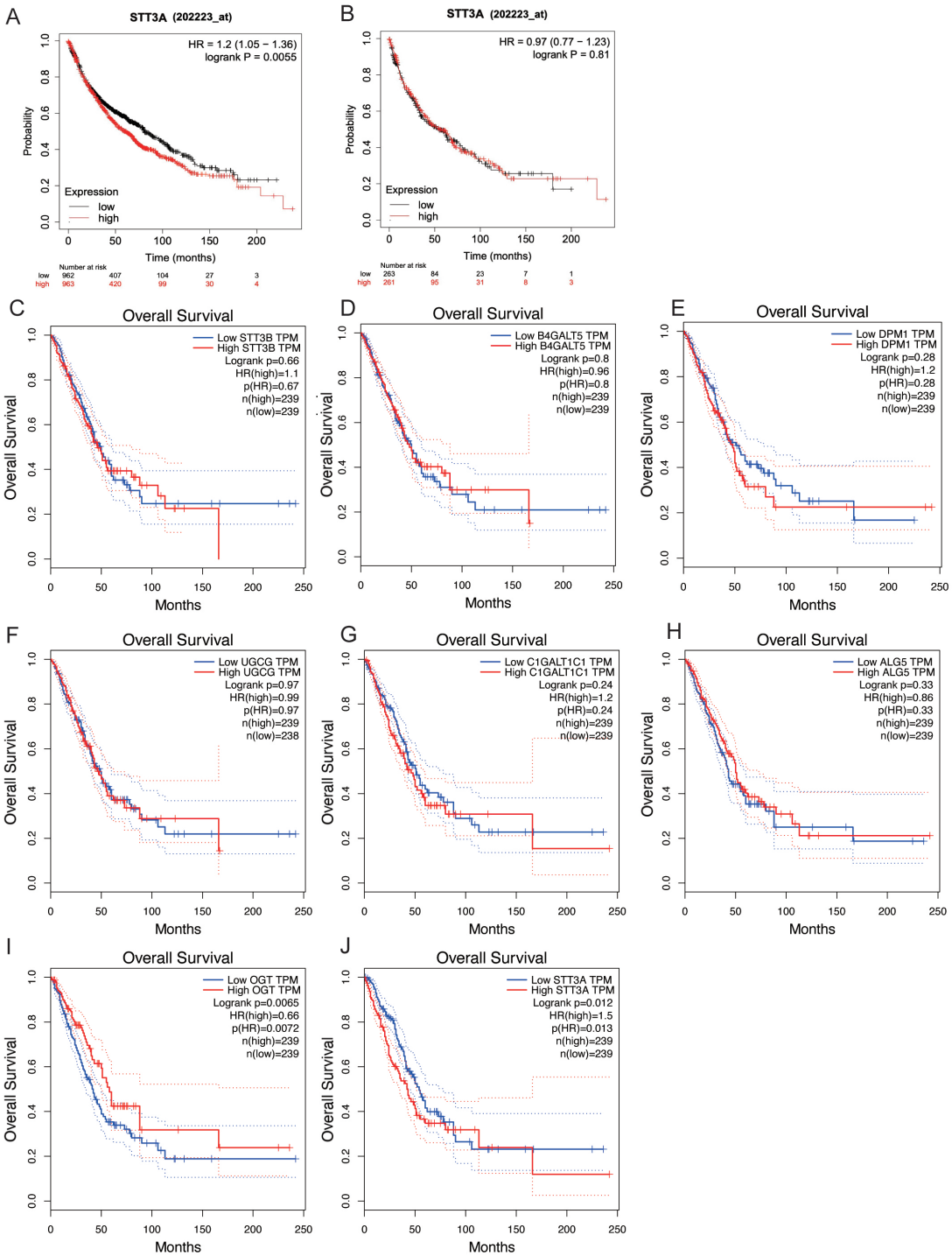

Figure S1 Correlation between expression level of DE glycosyltransferases and prognosis in non-small cell lung cancer. (A) Kaplan-Meier analysis of overall survival according to GEO database, STT3A high expression in NSCLC patients correlates with worse survival rate (P=0.0055). (B) In LUSC cohort, the expression level of STT3A is not correlated with prognosis (P=0.81). (C-H) According to the survival analysis of TCGA database, the expression levels of STT3B, B4GALT5, DPM1, UGCG, C1GALT1C1 and ALG5 were not related to the survival of LUAD patients. (I) OGT expression was inversely related to poor prognosis whereas (J) STT3A expression positively correlated with poor prognosis P=0.013). DE, differentially expressed; GEO, Gene Expression Omnibus; NSCLC, non-small cell lung cancer; LUSC, lung squamous cell carcinoma; TCGA, The Cancer Genome Atlas; LUAD, lung adenocarcinoma.

https://dx.doi.org/10.21037/tlcr-22-396

Table S1 Correlation between STT3A expression and clinicopathological variables in patients with lung adenocarcinoma

Variables	Number	STT3A expression		χ^2	P value
		High	Low		
All patients	183	92	91		
Gender				1.975	0.1599
Male	102	56	46		
Female	81	36	45		
Age				2.013	0.1559
<60 years	73	32	41		
≥60 years	110	60	50		
Tumor size				0.9501	0.3297
≤3 cm	68	31	37		
>3 cm	115	61	54		
Tumor location				0.1312	0.7172
Left	72	35	37		
Right	111	57	54		
Pathological grade				0.9588	0.3275
I & II	117	62	55		
III	66	30	36		
Lymph node				2.886	0.0893
Negative	89	39	50		
Positive	94	53	41		
Metastasis				3.084	0.0791
Negative	180	92	88		
Positive	3	0	3		
TNM stage				0.3082	0.5822
I & II	113	55	58		
III & IV	70	37	33		

https://dx.doi.org/10.21037/tlcr-22-396

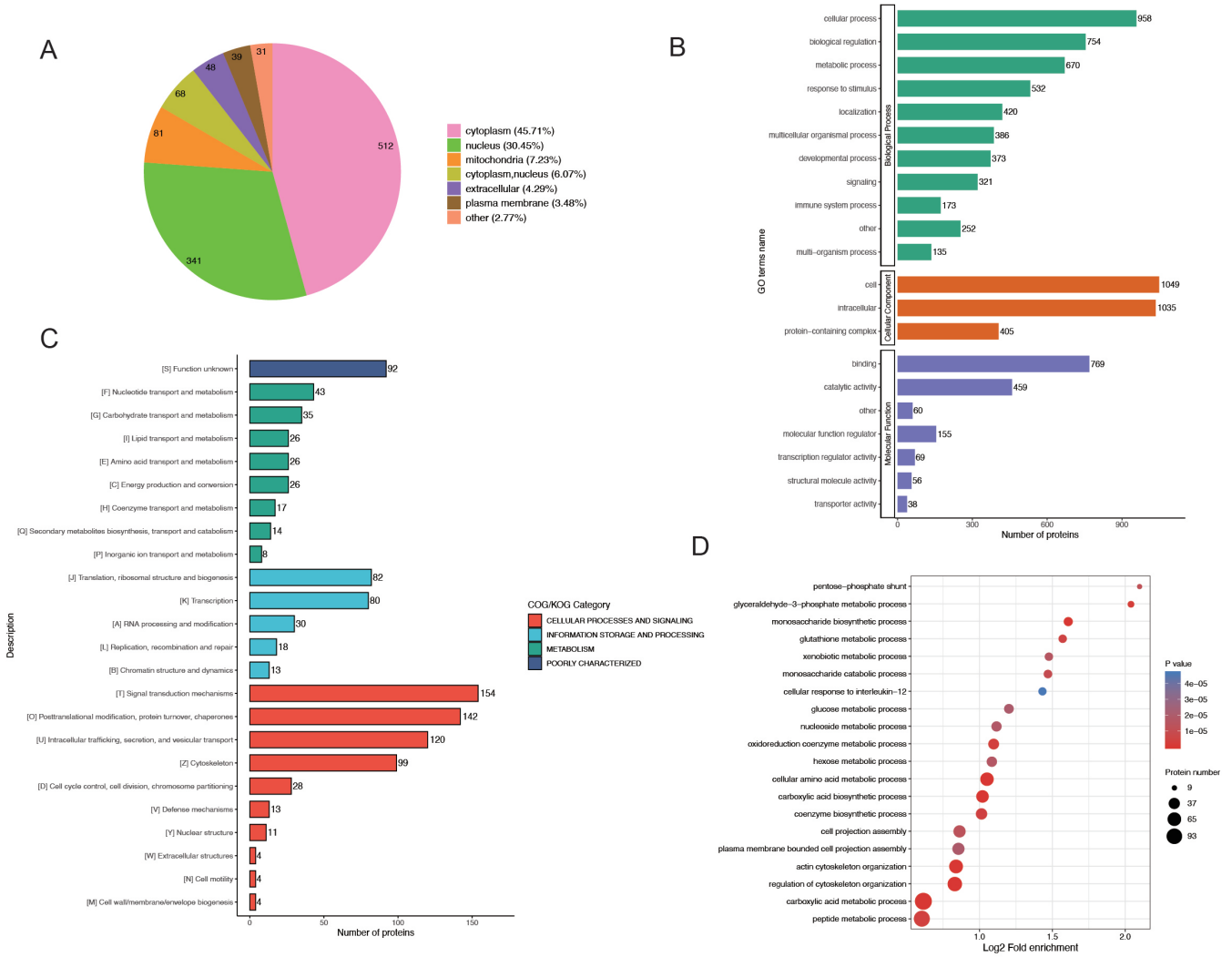

Figure S2 GO/COG analysis of down-regulated protein after STT3A deletion in PC-9. (A) The number of down-regulated proteins in each cell component. (B) GO enrichment analysis found down-regulated protein in biological process, cellular component and molecular function, and (C) COG analysis confirmed down-regulated changes in cell cycle and cell signaling pathway. (D) The down-regulated changes of GO analysis in BP are mainly concentrated in glucose metabolic process, plasma membrane bounded assembly and mitochondrial metabolism. GO, Gene Ontology; COG, Cluster of Orthologous Groups; BP, biological process.

https://dx.doi.org/10.21037/tlcr-22-396